Analyst

Electrodeposition behavior of homoleptic transition metal acetonitrile complexes interrogated with piezoelectric gravimetry

Journal:	*Analyst*
Manuscript ID	AN-ART-10-2019-001952.R1
Article Type:	Paper
Date Submitted by the Author:	12-Nov-2019
Complete List of Authors:	Sconyers, David; University of Kansas, Department of Chemistry Blakemore, James; University of Kansas, Department of Chemistry

ARTICLE

Electrodeposition behavior of homoleptic transition metal acetonitrile complexes interrogated with piezoelectric gravimetry

David J. Sconyers and James D. Blakemore*

Received 00th January 20xx,
Accepted 00th January 20xx

DOI: 10.1039/x0xx00000x

Homoleptic acetonitrile complexes of first-row transition metal ions are a common product of the detrimental speciation of coordination complexes and organometallic compounds. However, the electrochemical properties of such species are mostly unknown, introducing ambiguities into interpretation of electroanalytical data associated with studies of molecular electrocatalysis. Here, we have cataloged the cyclic voltammetric properties of the solvento complexes of Mn(II), Fe(II), Co(II), Ni(II), Cu(I), and Zn(II) in acetonitrile electrolyte, providing information on the cathodic electrodeposition and anodic stripping processes occuring with each ion. The electrochemical quartz crystal microbalance (EQCM) has been used to quantify these processes, as well as the rates of the *in situ* corrosion of electrodeposited materials by the strong organic acid dimethylforamidinium, $[DMFH]^+$. *Ex situ* X-ray photoelectron spectroscopic results confirm the interpretations of the voltammetric and gravimetric data, and confirm the periodic relationship between the metals. Taken together, the results described here provide an electrochemical roadmap useful in distinguishing currents arising from homogeneous electrocatalysis from currents associated with the redox cycling of secondary heterogeneous materials.

Introduction

The study of electrocatalytic processes for energy storage and/or conversion (e.g., proton reduction for the generation of H_2 or CO_2 reduction for production of liquid fuels) is a robust field, in part due to the importance of developing more sustainable industrial processes to power society.[1] Molecular metal complexes are attractive for studies of such processes, as they can be characterized by commonly available analytical techniques, are readily derivatized, and can be interrogated in solution for insights into their mechanisms of action. The earth abundant first-row transition metals are increasingly targeted for development of molecular catalysts, despite the challenges of ligand lability and propensity to undergo radical chemistry that they present to researchers in this area.[2]

In studies of molecular catalysis for energy conversion, isolated precatalyst species must often undergo activation by electrochemical reduction at a negatively polarized electrode surface in order to generate one or more active intermediates that react with substrates and eventually release the desired product(s). As most of the target reactions involve multiple electron and/or proton transfers, the operative catalytic mechanisms are often complex and multistep in nature.[3] Cyclic voltammetry and other electroanalytical techniques can probe these mechanisms, but information on the structure of intermediates or unexpected reaction side products is challenging to obtain from purely electroanalytical data.[4]

Department of Chemistry, University of Kansas, 1567 Irving Hill Road, Lawrence, Kansas 66045, USA. E-mail: blakemore@ku.edu; Tel: +1 (785) 864-3019
†Electronic supplementary information (ESI) available

Moreover, findings from a number of studies of molecular catalysis have revealed the challenges associated with speciation and/or decomposition of the molecular catalysts under electrochemical conditions. There is an emerging understanding that catalysts, exquisitely tuned through ligand design, are often rather sensitive to the operating conditions that are chosen for their use. In some examples, electrochemical activation of precatalyst materials results in formation of solid particles that function as the true catalytically active species.[5] In other cases, minor equilibria between active molecular catalysts and highly active secondary materials impact the analysis of catalyst performance since multiple species are in fact participating in product generation and energy conversion.[6]

In recent work, we have been developing techniques in which the electrochemical quartz crystal microbalance[7] (EQCM) is used to probe both molecular catalyst homogeneity[8] and the reactivity properties of transient heterogeneous materials that may form under conditions relevant to molecular catalysis.[9,10] In a series of control studies, we investigated degradation of two derivatives the well-known cobaloxime-type catalysts, which are capable of electrochemical hydrogen generation from organic acids. With EQCM measurements, we have shown that the cobaloximes can undergo demetallation under sufficiently acidic conditions, resulting in generation of a homoleptic cobalt acetonitrile complex, $[Co(NCMe)_6]^{2+}$, that serves as a precursor to formation of catalytically active heterogeneous material on the electrode surface. This material contributes to the majority of the observed activity of the nominally molecular cobaloxime catalysts.

A key finding from this cobaloxime work described above was assignment of the $[Co(NCMe)_6]^{2+}$ homoleptic complex as the

product of precatalyst speciation (via spectroscopic methods) and independent voltammetric and piezoelectric gravimetric studies showing that reduction of chemically prepared $[Co(NCMe)_6]^{2+}$ results in formation of heterogeneous cobalt(0) material on the electrode surface. Similar features appear in voltammetric and EQCM studies of both the pure $[Co(NCMe)_6]^{2+}$ and the acid-exposed cobaloximes, confirming involvement of this species in the observed catalyst system speciation under active, electrochemical conditions. The synthetic accessibility of the known homoleptic $[Co(NCMe)_6]^{2+}$ complex was especially helpful, since such a complex would be the logical product of ligand demetallation under the solvent/supporting electrolyte conditions (0.1 M NBu_4PF_6 in MeCN) typically used for electrochemical studies of molecular catalysts.

Imagining extension of these findings to other first-row transition metal systems, we have considered that decomposition pathways similar to those operating with the cobaloxime derivatives could operate in other molecular catalyst systems. This is particularly true in studies of reactions requiring addition of strong acids, since acid-promoted ligand loss can be anticipated to plague complexes of first-row transition metals. Appealingly, synthetic methods are available for isolation of homoleptic acetonitrile complexes of a variety of first-row transition metals, including Mn(II), Fe(II), Ni(II), Cu(I), and Zn(II).[11] On the other hand, we are not aware of any comprehensive studies aimed at probing the redox and/or EQCM gravimetric behavior of these homoleptic solvento species in common acetonitrile electrolyte; as these species are anticipated to be among the product(s) of speciation of a molecular catalyst, their redox properties have received less attention than they deserve. Notably, focused studies have appeared, however, on copper electrodeposition from organic solvento species in supercritical carbon dioxide ($scCO_2$) and under nonaqueous conditions that preclude H_2 generation.[12,13] Here, we report electroanalytical, EQCM, and spectroscopic investigations of homoleptic acetonitrile complexes of Mn(II), Fe(II), Ni(II), Cu(I), and Zn(II). The hexakis(acetonitrile) complexes of the +2 ions have been isolated and studied in all cases in the form of the tetrafluoroborate (BF_4^-) salts, except for the case of copper, which has been studied in the form of $[Cu(NCMe)_4]PF_6$. Cyclic voltammetry on both carbon and gold electrodes has been used to quantify the redox behavior of these systems, revealing information on the reduction potentials required for electron transfer and subsequent deposition of metallic solids. As in the case of prior work with cobalt, we find that a layer of transient, heterogeneous material forms following cathodic polarization of the electrode; in most cases, this material is entirely lost from the electrode surface over the course of a single cycle of voltammetry that includes potential excursion through visible anodic stripping features. Most of the deposited materials are also found, via EQCM and X-ray photoelectron spectroscopic studies, to be susceptible to chemical corrosion by the strong organic acid dimethylformamidinium triflate (pK_a = 6.1 in MeCN).[14] Taken together, these data provide a counterpoint to the known electrodeposition behavior of transition metal ions in aqueous solutions, as well as a practical roadmap for understanding how solvated metal ions may become involved in the chemistry of molecular (electro)catalytic systems.

Results

Synthesis and characterization

Synthesis of the homoleptic acetonitrile complexes of Mn(II), Fe(II), Co(II), and Ni(II) was carried out as described by Hathaway, Holah and Underhill.[11] Briefly, under dry and air-free conditions, metal powders or shavings undergo oxidation by treatment with nitrosonium tetrafluoroborate, $[NO]BF_4$, in acetonitrile solvent. Nitrous oxide gas (NO) generated by the oxidation of the metal and excess solvent present for the synthesis is then removed in vacuo to concentrate the solution. Cannula filtration of the concentrated solution to a fresh flask is followed by the addition of diethyl ether; this results in precipitation of the desired solvento metal dication tetrafluoroborate salts, which can be isolated following removal of excess solvent by cannula filtration and washing with ether. We attempted to prepare the $[Cu(NCMe)_4](BF_4)_2$ with literature methods, but obtained mixtures containing predominantly Cu^I on the basis of the observed solution color. Due to the challenge of purifying this mixture, we instead used the commercially available $[Cu(NCMe)_4]PF_6$ complex for further electrochemical work.

Solid state infrared spectra (see ESI, Figures S1 – S6) collected with the synthesized homoleptic complexes exhibit absorption features in close agreement with those previously reported for these complexes in the literature.[11] Notably, the position of a pair of strong nitrile C–N stretches at ~2300 cm^{-1} shifts from the value expected for free acetonitrile (2250 cm^{-1}), consistent with minor perturbation of the properties of MeCN upon coordination.[15] Alkyl C–H stretches at ~2900 cm^{-1} are also observed, consistent with the presence of the methyl groups in the coordinated MeCN ligands. A further signal near 1600 cm^{-1} was detected in a few cases, consistent with prior work on these complexes[11]; this signal is very weak in our experience, and is apparent only with the zinc and nickel complexes. It may be consistent with an unavoidable minor impurity of nitrosyl complexes, which could form during insufficient evacuation of the product NO gas from the reaction vessel following addition of $[NO]BF_4$.[16]

All of the prepared tetrafluoroborate salts are acutely moisture sensitive. Their hygroscopic nature is extreme, in that upon exposure to ambient atmosphere the material quickly develops a liquid layer surrounding the isolated powders (i.e., the materials may be deliquescent). This behavior is reflected in the infrared spectra, where in some cases the complexes present broad absorption bands near 3300 cm^{-1} which may be attributed to the presence of water. We have elected to handle and store the homoleptic complexes with the most rigorous possible air and water-free methods in an inert atmosphere glovebox; however, it appears that even over the timecourse of a few days under our strict conditions, the homoleptic complexes can act as dessicants in the trapping of trace moisture from rather hermetic environments. This is consistent

with their structure, and the loosely bound nature of the MeCN ligands.

Regarding the structure of the ions, prior work in the solid state has established the identity of the homoleptic complexes as $[Mn(NCMe_4]^{2+}$,[17] $[Fe(NCMe)_6]^{2+}$,[18,19] $[Co(NCMe)_6]^{2+}$,[20] $[Ni(NCMe)_6]^{2+}$,[21,22] $[Cu(NCMe)_4]^{+}$,[23,24] and $[Zn(NCMe)_6]^{2+}$.[25,26] However, it should be noted that the actual coordination environment could vary in homogeneous solution. Determination of the ligation of these first-row transition metal complexes is especially challenging due to their propensity to undergo ligand loss.[27] Minor thermal instability (on the order of 1-2% loss of solvent by gravimetry) has been observed at ambient pressures even below 100°C, resulting in the generation of secondary species containing motifs such as weakly coordinating counter ions or η^2-bound acetonitrile.[28] In summary, routine handling of these complexes is difficult. On the other hand, homoleptic complexes matching the spectral characteristics and stability profiles from the literature can be successfully isolated. With these materials in hand, we next turned to investigation of their electrochemical properties at carbon electrodes.

Electrochemical properties of the homoleptic metal ions

In all the cases discussed here, we find that the potentials required for the reduction of the homoleptic acetonitrile complexes fall within the working range accessible under typical conditions used in cyclic voltammetry on carbon electrodes. In dry acetonitrile solvent containing 0.1 M NBu_4PF_6 in MeCN, cathodic excursions as negative as –2.5 V vs. ferrocenium/ferrocene (denoted hereafter as $Fc^{+/0}$) can be readily performed under our conditions. Notably, this potential range is commonly used for studies of molecular catalysis, and thus our results generally confirm our hypothesis that the homoleptic solvento complexes could serve as precursors to heterogeneous materials if formed under the relevant conditions.

The voltammetry of the homoleptic complexes undergoing reduction/electrodeposition has a characteristic profile that is shared across the full series (Fig. 1). In the voltammetry, a single chemically irreversible two-electron reduction event (or, a one-electron event in the case of copper) is observed on scanning to a sufficiently negative potential. Within our working model, previously demonstrated for cobalt,[9] the M^+ or M^{2+} ion undergoes reduction to form transient reduced species that can participate in nucleation and growth of heterogeneous material on the electrode surface. Reduction-induced displacement of the weakly bound acetonitrile ligands no doubt contributes to this behavior; formation of lower-coordinate species can also promote ECE-type electrochemistry, in which transfer of two electrons at similar potentials is enabled by the intervening chemical step.[29] In the case of the systems studied here, the chemical processes involved in the reduction-induced behaviour are sufficiently fast that at modest scan rates (<250 mV/s) there are no signs of an oxidative feature at potentials near to that of the initial reduction. This suggests that the soluble reduced species are only present as short-lived transients which are quickly deposited as part of the growing mass of insoluble material. The sole exception to this is the behavior encountered for the cobalt complex (Fig. 1c), which exhibits a small oxidative feature ($E_{p,a}$ –1.14 V) near the reduction wave which likely arises from the re-oxidation of a transient Co(I) solvento species. Seemingly, the chemical step(s) involved in reorganization of the cobalt system following reduction is slower than the analogous reactions in the other systems.

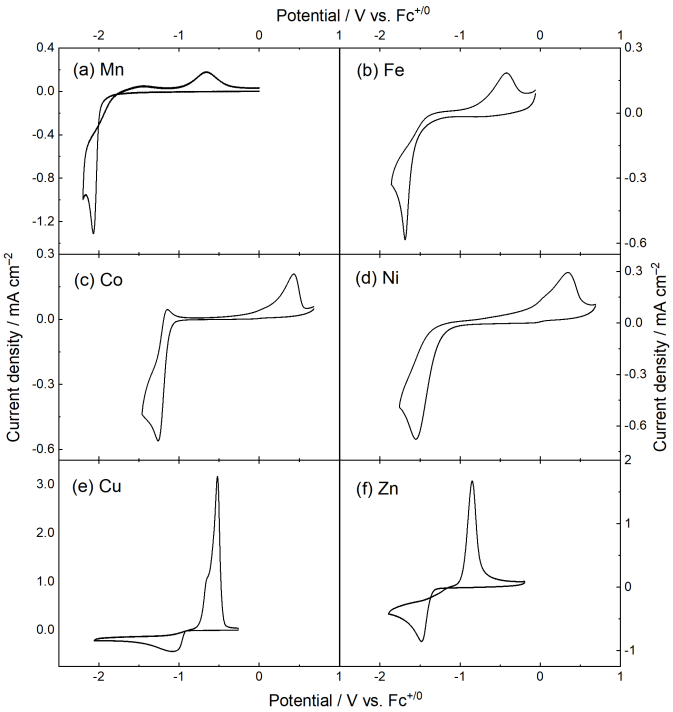

Figure 1. Cyclic voltammograms of the homoleptic acetonitrile complexes. Working electrode: highly oriented pyrolytic graphite (HOPG). Pseudoreference electrode: $Ag^{+/0}$. Counter electrode: platinum wire. All the experiments were carried out in solutions where $[M^{n+}]$ = 2 mM. Scan rate: 100 mV/s.

Manganese, copper, and zinc (Fig 1a, 1e, 1f) all display features at distinctive potentials that resemble the electrochemistry of metal ions involved in electrodeposition from aqueous electrolytes. Their reductions are particularly sharp, with notable "crossover" behaviors that appear upon reversal of the potential sweep following cathodic excursions in potential. There is a marked increase in the cathodic current flow between the forward and reverse sweeps, indicating that there has been a change in the composition of the electrode surface. This can be ascribed to more facile reduction of the homoleptic solvento complexes at electrodes featuring nucleated islands of solid metal, versus the rather inert pristine carbon electrode surface. However, this "crossover" behavior is not observed for all of the solvento complexes; iron, cobalt and nickel (Fig 1b, 1c, 1d) qualitatively share similar current-voltage responses and lack distinct crossover event that indicate a role for changes in the electrode surface in the chemistry occurring as a function of potential.

On the anodic sweep, all of the homoleptic complexes display a distinctive, broad, and symmetric feature attributable to the

two- or one-electron oxidation of electrodeposited material generated following reduction. The shape of the wave in all cases supports the identity of the material undergoing oxidation as heterogeneous and surface-bound in nature; this supposition is confirmed by the EQCM results discussed elsewhere (*vide infra*). We thus refer to this feature as an anodic stripping wave in all cases. Our working model proposes that passage through this anodic stripping wave results in regeneration of M^{+} or M^{2+} ions simultaneous with their liberation from the electrode surface as solvated species.

As the majority of work in electrodeposition of metal species has been carried out in aqueous conditions, we were interested to tabulate the potentials associated with reduction/deposition and oxidation/stripping in our system against the standard reduction potentials for aqueous metal ions in the oxidation states relevant to this study.[30] Table 1 shows the values for the cathodic peak potential ($E_{p,c}$), anodic peak potential ($E_{p,a}$), and average "midpoint" potential between these two values (E_{avg}). Also shown for comparison are the standard aqueous potential values (E^{o}) for the analogous M^{+2}/M^{0} couples in water. Examination of this data reveals no substantial trend between $E_{p,c}$ or $E_{p,a}$ and the standard potentials; this is consistent with significant contributions of kinetic influences and irreversibility to the single-wave peak potentials. On the other hand, there is a reasonable match in trend between E_{avg} (calculated as the mean of $E_{p,c}$ and $E_{p,a}$) and E^{o} for all the metals (except copper) discussed here; this may suggest that similar thermodynamic considerations drive the properties of the ion/metal systems in all the cases discussed here. For the apparently anomalous case of copper, inspection of the standard potentials[30] reveals the feature giving rise to its uniqueness in the series. Cu(I) is unstable and undergoes disproportionation in aqueous solution, since $E^{o}(Cu^{II/I})$ = 0.159 V and $E^{o}(Cu^{I/0})$ = 0.520 V; on the other hand, Cu(I) is stabilized and indeed isolable in acetonitrile.

Table 1. Potential values associated with the homoleptic ions and reference potentials for analogous aqueous metal ions under standard conditions.

Ion	$E_{p,c}$	$E_{p,a}$	E_{avg}	E^{o}
Mn(II)	–1.44	–0.03	–0.74	–1.18
Fe(II)	–1.06	+0.20	–0.43	–0.44
Co(II)	–0.63	+1.06	+0.22	–0.28
Ni(II)	–0.85	+0.97	+0.06	–0.26
Cu(I)	–0.43	+0.11	–0.16	0.52
Zn(II)	–0.83	–0.22	–0.53	–0.76

All standard potentials are reported in V vs. NHE. The position of the $Fc^{+/0}$ couple with respect to the NHE was assumed to be +0.63 V, based on an approximate conversion previously used in the literature.[31] Standard potentials[32] in aqueous solution (E^{o}) are from the standard tables.[30]

Addition of three equivalents (6 mM) of the strong organic acid dimethylformamidinium triflate ($DMFH^{+}$; pK_a = 6.1 in MeCN)[14] to the electrochemical cells containing the homoleptic metal acetonitrile complexes results in changes to the cyclic voltammetry profiles in each case (see ESI, Figs. S7-11). As an aside, we consider $DMFH^{+}$ as an especially useful strong organic acid, as it can be readily synthesized[33] from triflic acid in Et_2O and has a pK_a that is significantly lower than alternative acids such as anilinium triflate (pK_a = 10.6 in MeCN) or triethylammonium triflate (pK_a = 18.8 in MeCN).[34]

In the case of Mn(II) (see ESI, Figure S7), significant attenuation of the peak cathodic current is observed along with the appearance of a new reductive feature at more positive potentials. This may be the result of further speciation of the system, perhaps via coordination of dimethylformamide (DMF) to some of the population of Mn(II) species present in solution. In addition, the the voltammetric features of the system are significantly broadened, suggesting decreased electrochemical reversibility and attenuated electron transfer kinetics for all the processes involved. Further consistent with this notion, the anodic stripping wave is shifted to more positive potentials by ca. 0.5 V in the presence of acid.

In the case of Fe(II) (see ESI, Figure S8), the voltammetry in the presence of three equivalents of acid lacks an appreciable anodic stripping wave but retains a significant cathodic process similar to the case without acid present. On the basis of this profile and our prior work examining the cobalt(II) system,[9,10] this behaviour can be attributed to rapid chemical corrosion of the electrodeposited iron during the voltammetric experiment. In this situation, corrosion occurs rapidly when the nascent iron(0) material is not cathodically protected ($E_{app} \geq -1.6$ V) but prior to reaching the threshold potential required to observe anodic stripping ($E_{p,a}$ = –0.42 V). This temporal balance of ineffective cathodic protection is, in part, a consequence of the modest scan rate used (100 mV/s). However, scan rates on this order are most common in molecular catalysis research, and therefore we have focused on that regime here. Finally, minor enhancement of the reductive current associated with the single cathodic process observed for Fe(II) is observed, an appearance that suggests a possible role of Fe(0) in catalytic or pseudo-catalytic generation of hydrogen gas. In any case, Fe(0) on the carbon electrode surface can be seen to react quickly with $DMFH^{+}$.

Exposure of the homoleptic Ni(II) complex to three equivalents of $DMFH^{+}$ for cyclic voltammetric studies (see ESI, Figure S9) results in similar reductive chemistry to that observed in experiments that lack acid. However, the anodic stripping wave for the metallic nickel formed on the electrode surface is retained in the voltammetry despite modest current enhancement to the reductive wave. This suggests that electrodeposited nickel is more resilient to chemical corrosion than iron, which is borne out in the gravimetric data described later (*vide infra*). It is also consistent with the apparently more reducing nature of Fe(0) vs. Ni(0) ($E_{p,c}$ = –1.68 vs. –1.55 V, respectively).

Cu(I) exhibits attenuated oxidative current associated with its anodic stripping feature following treatment of the system with acid for voltammetry (see ESI, Figure S10). This situation is in agreement with similar arguments made earlier regarding the occurrence of chemical corrosion at potentials where the nascent heterogeneous Cu(0) material is no longer cathodically protected. Our prior work with the cobalt system examined this phenomenon in detail, and confirmed that corrosion, an acid- and time-dependent process, does impact voltammetric

profiles across variations in scan rate, potential sweep width, etc.[10]

The voltammetry of Zn(II) in the presence of three equivalents of $DMFH^+$ (see ESI, Figure S11) is nearly identical to that observed without acid, with only minor current enhancement and virtually no changes in the appearance of the anodic stripping wave. This suggests that the electrodeposited zinc metal is relatively stable, with little material undergoing chemical corrosion processes during the window where the nascent zinc(0) is not cathodically protected.

Voltammetric properties interrogated by piezoelectric gravimetry

The inferences made in the preceding section regarding formation of heterogeneous material on the electrode surface can be directly confirmed and studied further by use of the electrochemical quartz crystal microbalance (EQCM). An EQCM, useful for carrying out piezoelectric gravimetry in real-time during electrochemical experiments, relies on the converse piezoelectric effect to monitor the apparent mass of the working electrode.[7] The electrodes used here were AT-cut quartz crystals sputtered with gold, which serves as the electroactive surface in contact with the solution for voltammetric studies. Using the Sauerbrey equation,[35] we can relate the readily measured vibrational frequency change of the quartz disk to an apparent change in mass. We have previously leveraged the high sensitivity of this technique to quantify the formation and properties of heterogeneous material arising during molecular electrocatalysis, and can routinely measure mass changes on the order of ±5 ng (±5 Hz).[9,10]

Generally speaking, the voltammetric profile of the homoleptic metal complexes at a gold working electrode closely resembles that of the complexes at a carbon electrode. A single major cathodic and anodic wave are measured in each case, corresponding to electrodeposition and stripping, respectively. The gravimetric data from simultaneous EQCM monitoring during voltammetry confirm generation of heterogeneous, electrode-bound material at sufficiently negative potentials to carry out reduction of the homoleptic metal complexes. Stated another way, onset of current corresponding to reduction of the $[M(NCMe)_n]^{m+}$ complexes corresponds with the onset of mass deposition and increasing mass of the electrode. Mass continues to deposit at all potentials negative of the onset, including during both the cathodic and anodic sweeps of the voltammetry.

Qualitative variations of this behavior pattern distinguish the Co(II), Ni(II), Cu(I), and Zn(II) complexes in EQCM studies (see Figure 2). For analogous 2-mM solutions containing the latter three ions, ca. 425 ng of solid are deposited during typical cyclic voltammograms. Notably, the system with Co(II) appears to deposit significantly more mass, ca. 800 ng; we suspect this may be due to surface trapping of significant quantities of solvent or supporting electrolyte. Electron transfer to the Zn(II), Cu(I), and Co(II) ions seems rapid, on the basis of rather sharp reduction waves in each case. On the other hand, the reduction of the Ni(II) complex is broad and bifurcates into two distinct waves at the gold electrode; this may be ascribable to unique interactions between the Ni(II) system and the gold electrode, considering mass deposits during both cathodic processes. Similarly, multiple overlapping contributions are apparent in the anodic stripping wave for the Zn system—this profile is considerably more complex than the behavior encountered for the carbon electrodes, and suggests unique interactions and/or deposition of unique zinc species on gold.

As anticipated from the behavior of the systems on carbon electrodes, passage of the applied potential through the symmetric anodic waves results in loss of virtually all the new mass deposited during the cyclic voltammetry experiment. Thus, extension to multiple cycles shows negligible change in electrode mass over time. Connecting to studies of molecular catalysis, this finding suggests that both EQCM studies and careful interpretation of electroanalytical features present in the voltammetric data are needed to implicate involvement of the homoleptic solvento species in observed reactivity. No significant solid material is anticipated to remain on the electrode following voltammetric redox cycling of the homoleptic Zn(II), Cu(I), Ni(II), and Co(II) ions.

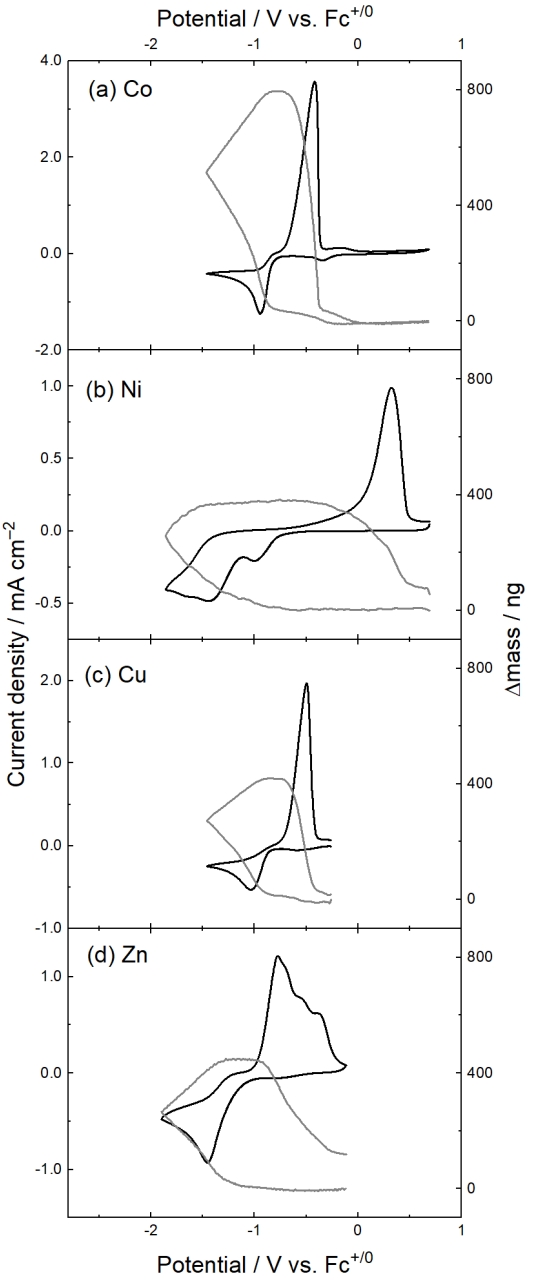

Figure 2. EQCM studies of homoleptic cobalt, nickel, copper and zinc acetonitrile complexes.. Potential-dependent current (black lines) and gravimetric mass data (gray lines) are shown for four species. Working electrode: gold-sputtered quartz disc. Pseudoreference electrode: $Ag^{+/0}$. Counter electrode: platinum wire. All electrochemistry carried out in solutions where $[M^{n+}]$ = 2 mM. 100 mV/s scan rate.

Surprisingly, the situation regarding deposition/stripping of mass from the electrode for Mn(II) and Fe(II) as studied by EQCM is quite different from the other cases (see Figure 3). For Mn(II), the generation of heterogeneous material implied by the electroanalytical work is confirmed by the EQCM. Namely, the $[Mn(NCMe)_6]^{2+}$ species undergoes reduction on gold at $E_{app} \leq -2.20$ V, leading to formation of heterogeneous material. A paired anodic wave is seen, and similar to the case of carbon (see Figure 1a) could be assumed to lead to stripping of manganese material off the electrode surface. However, the gravimetric EQCM data in Figure 2a show that passage of the potential through the anodic "stripping" feature is not associated with any mass change at the electrode surface. This finding, reproducible across multiple experiments and several unique runs, suggests that the anodic feature merely changes the oxidation level of the surface-bound material. Thus, upon multiple cycling, mass aggregates at the electrode.

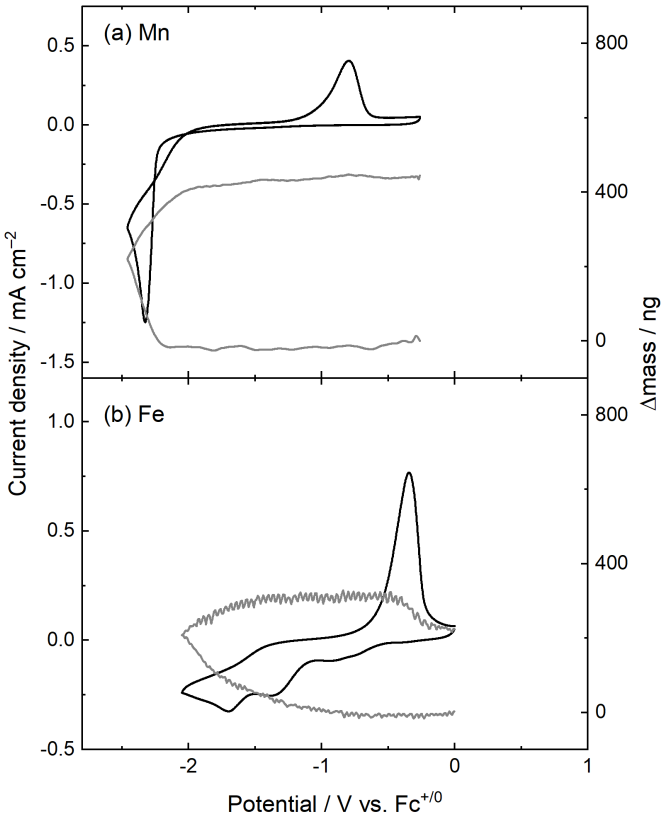

Figure 3. EQCM studies of homoleptic manganese and iron acetonitrile complexes.. Potential-dependent current (black lines) and gravimetric mass data (gray lines) are shown for both species. Working electrode: gold-sputtered quartz disc. Pseudoreference electrode: $Ag^{+/0}$. Counter electrode: platinum wire. All electrochemistry carried out in solutions where $[M^{n+}]$ = 2 mM. 100 mV/s scan rate.

A similar situation to that of Mn is encountered for the Fe system on gold electrodes as studied by EQCM (see Figure 3b). Specifically, electroreduction of $[Fe(NCMe)_6]^{2+}$ leads to formation of solid material on the electrode surface. However, passage of the applied potential through the anodic "stripping wave" leads to only a minor drop in the electrode mass. This, like the case of Mn, suggests that internal redox cycling of the surface-attached metal material is occurring, rather than oxidation followed by dissolution of the solid layer to regenerate $[Fe(NCMe)_6]^{2+}$. This behavior does not seem to be affected by the speciation or electron transfer properties of the homoleptic solvento complexes, as the Mn system displays fast electron transfer as judged by the voltammetry data on gold, whereas the Fe system shows multiple, apparently slower reduction events, much like the case of Ni shown in Figure 2b). Only minor variability in the voltammetric features is observed across multiple cycles of electrochemistry with the homoleptic

acetonitrile complexes. Following the first scan, there are minor shifts (<80 mV) in the onset potential of reduction during the cathodic excursions as well as in the onset of the oxidative features during the anodic return sweep. This is readily attributable to changes in the gold surface following nucleation of deposited metal, with the consequence that deposition or anodic stripping may be influenced by the composition of the working electrode, which varies from scan to scan.

Comparison of the actual mass deposited (as measured by EQCM) and the theoretical mass change (based on charge passed for formation of M^0) reveals similar values across multiple cycles as well. However, Fe, Ni, and Zn show relatively high efficiency for M^0 formation at 80% whereas Mn and Cu show lower efficiencies of 45-60%. This suggests reduced forms of the metal may be soluble and diffuse away from the electrodes prior to precipitation.

Fundamentally, generation of the solid heterogeneous M(0) materials in each case discussed here involves a multistep process. For Mn(II), Fe(II), Co(II), Ni(II), and Zn(II) transfer of two electrons and an unknown number of discrete chemical steps may be involved in the formation of the heterogeneous material. To further investigate the potential dependence of the formation of heterogeneous material, and to interrogate for vestiges of the two overlapping one-electron reduction processes that must be involved, we analyzed the mass data collected during cyclic voltammetry more deeply. Specifically, we carried out mathematical differentiation of the change in mass versus time data. The resulting plots of $d\Delta m/dt$ versus time (see ESI, Figures S17 to S26) show, in general, only a single regime of accelerating mass deposition as the applied potential is swept to increasingly negative potentials during the cathodic excursions. This is true for Mn, Fe, Ni, and Cu in the present work. We interpret the appearance of the $d\Delta m/dt$ data as indicating a single zone of increasing mass deposition rate (as electron transfer accelerates at more negative applied potentials) followed by a zone of decelerating mass deposition due to the inevitable depletion of the starting homoleptic ions from the reaction-diffusion layer near the working electrode. The appearance of the data here for Mn, Fe, Ni, and Cu is reminiscent of that previously collected by our group for Co species.[10]

The $d\Delta m/dt$ versus time data for Zn(II) are unique, and indicate the involvement of at least three zones in apparent mass increases at the electrode. In addition to the two discussed above, there is an addition plateau-like region that we hypothesize may suggest (i) dynamics within the electrodeposited material and/or formation of multiple surface species or (ii) diminished depletion of the starting Zn(II) species from the reaction-diffusion layer. The observation of multiple overlapping anodic stripping features for the deposited Zn material (see Figure 2d) may support the former theory, but further work will be needed to distinguish the details of this more complex case.

Chemical corrosion interrogated by piezoelectric gravimetry

Addition of three equivalents of $DMFH^+$ acid to the EQCM experiments with the homoleptic ions results in changes in the voltammetric and gravimetric profiles that are consistent with the model proposed here to explain the behavior of these systems (see Figures S12-S16 in ESI). However, an interfering feature that impacts clear interpretation of the potential-dependent mass and current data lies in the tendency for the reaction-diffusion layer near the working electrode to become depleted of $DMFH^+$ over the course of the cyclic experiment. We anticipate this may occur due to the significant background currents corresponding to gold-catalyzed hydrogen generation measured in our prior work.[9]

Therefore, for this study, we have focused on direct quantification of chemical corrosion rate induced by three equivalents of $DMFH^+$ (on the basis of added homoleptic complex in the working electrolyte solution) for each of the electrodeposited materials by an alternative approach. Specifically, we have carried out linear sweep voltammetry over the range of potentials used in the other relevant cyclic experiments (see Figure 2 and 3). Following completion of the LSV, however, the EQCM was used to continue monitoring the mass of the electrode while sitting at open circuit following completion of the applied potential program of the LSV. The resulting mass data are shown in Figure 4, and in Figures S27-S29 in the ESI.

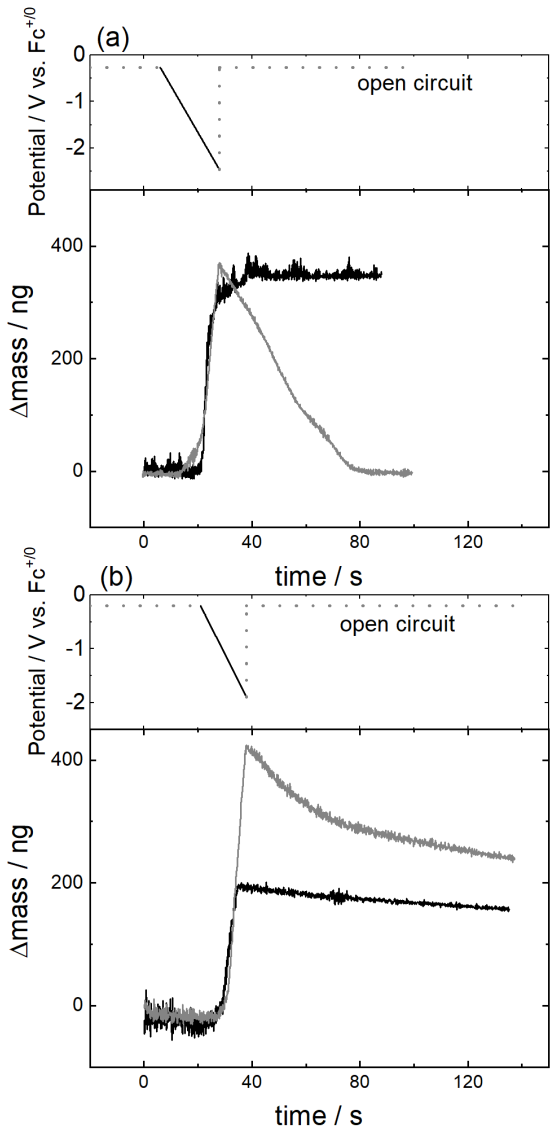

Figure 4. Corrosion of heterogeneous material generated from reduction of the homoleptic manganese and zinc acetonitrile complexes. Gravimetric data is shown for times before, during, and after the cathodic linear sweep voltammetry experiments were performed on the molecular precursors, over the range of potentials shown in Figures 2 and 3. (a) Manganese gravimetric data. Upper panel: Applied potential as a function of time during LSV. Lower panel: Black line, mass profile of electrode immersed in a solution of manganese solvento complex; Gray line, mass profile of electrode immersed in solution of manganese complex and 3 equiv. $DMFH^+$. (b) Zinc gravimetric data. Upper panel: Applied potential as a function of time during LSV. Lower panel: Black line, mass profile of electrode immersed in a solution of zinc solvento complex; Gray line, mass profile of electrode immersed in solution of zinc complex and 3 equiv. $DMFH^+$. Mass loss indicates surface-bound material instability or chemical corrosion. Working electrode: gold-sputtered quartz disk. Pseudoreference electrode: $Ag^{+/0}$. Counter electrode: platinum wire. All electrochemistry carried out in solutions where $[M^{n+}]$ = 2 mM. 100 mV/s scan rate.

In all of the cases measured here, the steep gain in apparent electrode mass at early times corresponds to the LSV-driven deposition of mass on the electrode surface. The period following that rise in mass corresponds to a condition in which the nascent heterogeneous material is immersed in the working solution, a situation in which it could undergo chemical corrosion. For the Mn system (Figure 4a), nearly identical mass is deposited (ca. 375 ng) both without and with 6 mM $DMFH^+$ added, suggesting that acid does not impact the chemistry leading to metal deposition. However, the $DMFH^+$ present in the solution corrodes the nascent metal off the surface, as judged by the rapid loss of mass (–9 ng s^{-1}). This is quite rapid, and contrasts with the virtually indefinite stability of the Mn(0) in the absence of acid (Figure 4a, black line). The behavior of the Zn system (Figure 4b) offers an interesting counterpoint to these findings with the Fe system. Specifically, nearly 2x mass is deposited in the case with $DMFH^+$ added, suggesting that Zn–H species may accelerate mass deposition in this case. Furthermore, two regimes of mass loss (–4.3 and –0.7 ng s^{-1}) are observed for the $DMFH^+$-promoted corrosion; this is consistent with our other findings, in that multiple species may be present on the electrode surface following electrodeposition and show differential tendencies toward chemical corrosion.

Related findings were made for the other ions in this study (see ESI for details). Nickel showed a minor enhancement of electrodeposition in the presence of acid, and undergoes two regimes of rather rapid corrosion with acid (–1.7 and –0.1 ng s^{-1}). On the other hand, mass deposition from reduction of the homoleptic Fe(II) complex in the presence of $DMFH^+$ is mildly attenuated by ca. 80 ng. However, the electrodeposited iron(0) does react quickly with acid to corrode off the surface (–2.0 ng s^{-1}). Finally, copper also appear to undergo rapid corrosion by acid (–2.0 ng s^{-1}). All these results are summarized in Tables 2 and 3, including both the apparent masses deposited in each case as well as the corrosion rates with and without acid added.

Table 2. Quantification of mass deposition from homoleptic acetonitrile complex precursors.

Ion	Mass deposited without acid (ng)	Mass deposited with acid (ng)
Mn(II)	446	483
Fe(II)	320	260
Co(II)	795	727
Ni(II)	380	598
Cu(I)	417	469
Zn(II)	450	531

Total mass deposited in the absence of acid determined from cyclic voltammetry detailed in Figures 2 and 3. Mass deposited with acid present determined from Figures S12-16.

Table 3. Quantification of electrodeposited material corrosion rates.

Ion	Corrosion rate without acid (ng s^{-1})	Corrosion rate(s) with acid (ng s^{-1})	Overpotential for H_2 generation (η)
Mn(II)	–0.12	–9.0	0.98
Fe(II)	–0.01	–2.0	0.67
Co(II)	–0.40	–2.2	0.02
Ni(II)	–0.05	–1.7, –0.14	0.18
Cu(I)	–0.20	–2.8	0.40
Zn(II)	–0.30	–4.3, –0.72	0.77

Corrosion rates with and without 3 equiv. $DMFH^+$ determined by calculation of the slope from a linear fit of the linear sweep voltammetry data in Figure 4 as well as Figures S27-29. The final column is the calculated overpotential of each system, based upon the reversible thermodynamic potential of the dimethylformamidinium-based H_2 evolution reaction ($E^{o'}(H^+/H_2)$ = –0.39 V vs. $Fc^{+/0}$ and the value of E_{avg} in V vs. $Fc^{+/0}$.[14]

Examination of the overpotential for H_2 evolution (Table 3) for each of the heterogeneous deposits reveals a distinct periodic trend across the first-row transition metals. The thermodynamic driving force for hydrogen generation decreases from a maximum in the series for manganese until reaching cobalt. The trend then reverses direction and shows an increasing driving force going across the series of nickel, copper, and finally zinc. Plotting the observed corrosion rate with $DMFH^+$ present as a function of the estimated overpotential (Figure 5), reveals that (i) increased rates of corrosion correlate with high apparent overpotentials and (ii) the rates of corrosion are reasonably comparable for all the transition metals studied here. In line with expectations from thermodynamics, the more reducing materials facilitate more rapid proton reduction. Assuming that these systems are behaving in a Nernstian fashion, we note here that the free energy change for hydrogen evolution follows a reasonable trend; hydrogen evolution is significantly more exothermic driven by Mn^0 than Co^0 (for example), and thus the process is faster for Mn^0 than Co^0.

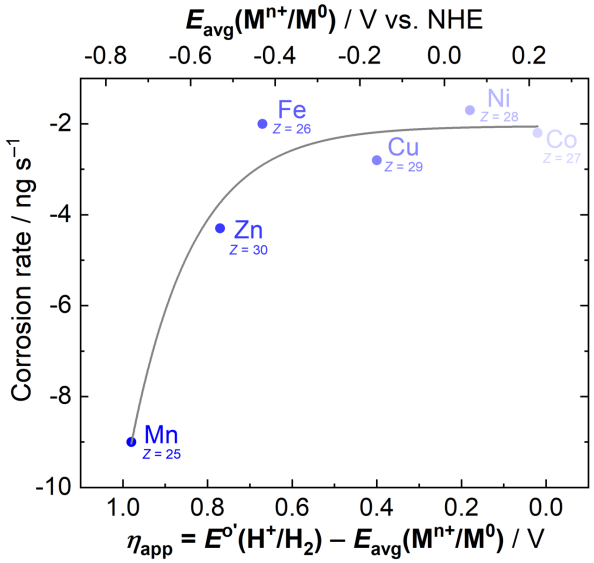

Figure 5. Correlation of the observed corrosion rates measured from the EQCM LSV experiments with the estimated overpotential for H_2 generation in acetonitrile for the electrodeposited metal species. Corrosion was induced by treatment with three equivalents of dimethylformamidinium triflate as described in the main text. The gray trend line is intended only to guide the eye. The position of the $Fc^{+/0}$ couple with respect to the NHE was assumed to be +0.63 V, based on an approximate conversion previously used in the literature.[31]

X-ray photoelectron spectroscopic studies

In order to confirm that the electrodeposition processes measured by piezoelectric gravimetry indeed correspond to formation of heterogeneous metal(0) solids, X-ray photoelectron (XP) spectra were collected. In order to prepare the samples for interrogation by XP spectroscopy, 1 cm^2 electrodes were polarized at the $E_{p,c}$ values measured for each ion previously on carbon, immersed in 2 mM solutions of the homoleptic solvento species for 5 min. Following the electrodeposition, the electrodes were rinsed thoroughly with dry acetonitrile and packaged for transport to the XP spectrometer. Notably, the samples were exposed to ambient conditions (air, water) for loading into the XP spectrometer, and thus the nascent metal(0) material could be found in oxidized forms. The XP data are summarized in Figure 6.

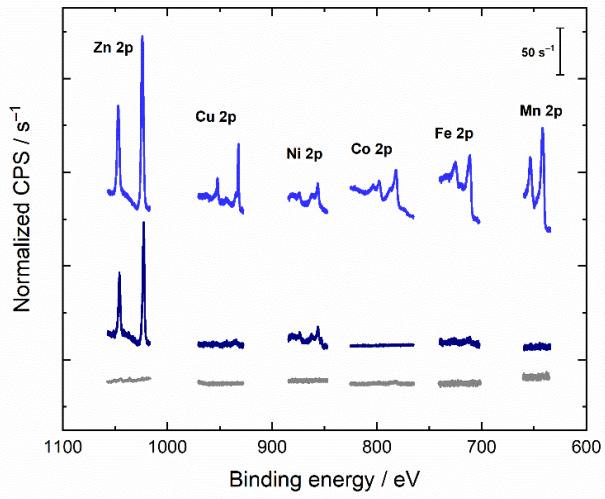

Figure 6. X-ray photoelectron spectroscopy of electrodeposited material. High resolution data are shown for regions in the spectra which correspond to the energies required to eject electrons from M 2p orbitals. 1 cm^2 HOPG carbon blocks served as the electrode surfaces for sample preparation. They were subsequently immersed in a 2 mM solution of a given homoleptic acetonitrile complex and polarized at $E_{p,c}$ for the species for 5 min. The upper (blue) line details the spectra for the electrodeposited material. The middle (dark blue) line shows the spectra of similarly prepared electrodes followed by 5 min immersion in 6 mM $DMFH^+$. The bottom (gray) line are blanks for the regions collected on a clean, bare carbon surface.

Survey spectra collected for the electrodes prepared with deposited material show signals in each case corresponding to the expected metal, as well as oxygen, nitrogen, phosphorus, and fluorine. All the electrodes, including a control blank electrode not subjected to any electrodeposition, show the presence of carbon and a small amount of oxygen arising from adventitious adsorbed water and minor oxidized carbon species. These are consistent with electrodeposition of relatively thin layers of metal in each case, as carbon signals are clearly present after electrodeposition; the signals from phosphorus and fluorine can be understood to arise from trapped $Bu_4N^+PF_6^-$ on the surface as well. Moreover, contributions from M(0) species were not observed with any of the electrodes, suggesting complete oxidation upon air exposure.

The nature of the deposited metal material was investigated by collection of high resolution M 2p spectra, shown as the upper blue lines in Figure 6. In each case, strong M $2p_{3/2}$ and $2p_{1/2}$ photoelectron signals were observed (plus paramagnetic satellites in some cases, see ESI), consistent with significant electrodeposition of the metal on the electrode surface during cathodic polarization. Comparing between the samples, the M 2p signals obey the expected periodic trends, in that the binding energy increases with increasing atomic number (*Z*). In addition, the relative sensitivity factors (RSF) are also *Z*-dependent; thus, the data in Figure 6 are normalized by standard Scofield RSF values for clarity.[36] On the basis of the M $2p_{3/2}$ peak binding energy values, the dominant material on the surface of each electrode was found to be ZnO, Cu_2O, Ni_2O_3, possibly CoOOH or Co_2O_3, Fe_2O_3, and Mn_2O_3, respectively.[36] These findings are consistent with the air exposure of the samples prior to data collection, and moreover, confirm that metal(0) species are the most likely primary product of the electrodeposition processes in each case.

Additional high resolution data were collected in the N 1s region, in order to investigate the nature of the nitrogen species present on the surface. In principle, there are two possible N-containing species that could be found on the surfaces: N arising from bound or trapped acetonitrile (expected to appear with a binding energy ca. 400 eV) or N arising from trapped tetrabutylammonium cations present in the electrolyte (binding energy expected ca. 402-403 eV).[37] In all the high resolution N 1s data (see ESI, Figures S33, S36, S39, S42, and S45), we find signals in the range of 402.5-403 eV that are thus consistent with inclusion of Bu_4N^+ in the deposited materials. The presence of Bu_4N^+ may also be attributable to incomplete rinsing to remove the supporting electrolyte from the presumably high surface area particulate materials on the electrode surface following electrodeposition.

XP spectra were also collected on identical carbon electrodes prepared with electrodeposited material but following immersion in a solution containing 6 mM $DMFH^+$ for 5 min. The resulting data are summarized in the dark blue lines in Figure 6. In the cases of Mn, Fe, Co, and Cu, the data are consistent with effective corrosion of virtually all the electrodeposited material from the surface. Thus, in the XP spectra, there are practically no signals corresponding to the presence of the respective metal ions on the surface. The Ni 2p and Zn 2p data, however, suggest that those metals were not completely corroded off the electrode surface by the excess $DMFH^+$ over the timecourse of the 5 min immersion carried out prior to XP analysis. These findings agree with those for Ni and Zn from the quantitative piezoelectric gravimetry study (*vide supra*); namely, only Ni and Zn show multiphase corrosion behavior with $DMFH^+$. Taken together with the XP data, these findings suggest that multiple forms of Ni(0) and Zn(0) species form under the relevant electrodeposition conditions, and that one or more of these may be resistant to corrosion. As a result, significant Zn and Ni remain on the electrode following exposure to corrosive conditions.

Discussion

In this study, we have interrogated the electrodeposition properties of a group of homoleptic first-row transition metal ions that are probable species that could result from speciation of molecular electrocatalysts. The electrochemical and piezoelectric gravimetric data confirm our initial hypothesis that these ions can indeed undergo electrodeposition at the moderate to strongly reducing potentials in acetonitrile electrolyte that are relevant to studies of molecular catalysis. Thus, they could contribute to formation of heterogeneous material during reductive redox cycling of a molecular catalyst, and could contribute to either productive or parasitic reactions and impact the energy conversion efficiency of a system built from the relevant components. The new electroanalytical data collected here for the first time provide the key current-voltage features for the research community that will be useful in

anticipating the formation of undesired heterogeneous materials from tailored molecular precursors.

However, as we have found in our prior work focusing solely on cobalt, the EQCM approach reveals that the heterogeneous material formed by electrodeposition is not static in its behavior. Rather, in most of the cases studied here, heterogeneous materials form and dissolve back into solution on the timescale of single cyclic voltammetry experiments. Most troublingly, the heterogeneous materials formed during catalysis would not be detectable by *ex situ* methods, due to the propensity of the deposited material to either (a) undergo electrochemical oxidation via anodic stripping or (b) undergo chemical corrosion by even short exposure to working solutions containing moderate to strong acids. This process occurs on the minutes timescale in all cases studied here, thus leaving only a short window where the transient heterogeneous species can be observed.

On the basis of the XP spectra, the materials formed on the electrode surface are complex in nature. Formed under the kinetically-controlled conditions of electrodeposition by cyclic voltammetry, there are likely multiple "types" of species on the surface, corresponding to nucleated metal islands, particle agglomerations, and/or small clusters. These features are now known to take up some quantity of the tetrabutylammonium ion present in the electrolyte. Thus, the nature of the surface-bound material remains elusive. Notably, we anticipate that further work in this area could both improve analytical methods for detection of catalyst system speciation products, as well as improve the body of knowledge in strategies for preparation of improved catalysts. In our own work, we are also pursuing further studies of the heterogeneous materials formed by electrodeposition in nonaqueous media.

Conclusion

The homoleptic acetonitrile complexes of the first-row transition metal ions Mn(II), Fe(II), Co(II), Ni(II), Cu(I), and Zn(II) are precursors for electrodeposition of heterogeneous metal materials in acetonitrile electrolyte. EQCM studies, in concert with *ex situ* XP spectroscopy, confirm electrodeposition of the ions and provide quantitative insights into the reactivity profiles of the electrodeposited species. As found in aqueous conditions, the solid metal electrodeposits are not noble and undergo corrosion when exposed to strong acid. Unlike the case of aqueous solutions, however, use of dry acetonitrile enables virtually total exclusion of protic reagents and thus completely independent study of anodic stripping and chemical corrosion. Both these processes can impact studies of molecular catalysis, and the powerful electroanalytical technique of piezoelectric gravimetry (enabled by use of the EQCM) is uniquely poised to distinguish the roles of these processes in molecular catalysis research and in studies of transient heterogeneous materials.

Experimental Section

General considerations

All manipulations were carried out in dry, N_2-filled gloveboxes (Vacuum Atmospheres Co., Hawthorne, CA) or under a N_2 atmosphere using standard Schlenk techniques unless otherwise noted. All solvents were of commercial grade and dried over activated alumina using a PPT Glass Contour (Nashua, NH) solvent purification system prior to use, and were stored over molecular sieves. All chemicals were from major commercial suppliers and used after extensive drying. $[NO]BF_4$ was dried in vacuo overnight. Protonated dimethylformamide ($[DMFH]^+[OTf]^-$), was synthesized by the method of Favier and Duñach.[33] $[Mn(MeCN)_4][BF_4]_2$, $[Fe(MeCN)_6][BF_4]_2$, $[Co(MeCN)_6][BF_4]_2$, $[Ni(MeCN)_6][BF_4]_2$ and $[Zn(MeCN)_6][BF_4]_2$ were prepared according to procedures in the literature.[11] $[Cu(MeCN)_4][PF_6]$ was purchased and dried *in vacuo* for 12 h at room temperature prior to use (Sigma Aldrich).

Spectroscopic instruments and methods

Infrared spectra were recorded on a Shimadzu IRSpirit FTIR spectrometer at room temperature located within an inert atmosphere glovebox. Solid samples of the isolated homoleptic acetonitrile complexes were characterised on this instrument using the QATR-S single-reflection attenuated total reflectance (ATR) measurement attachment without further preparation.

X-ray photoelectron spectroscopy (XPS) X-ray photoelectron spectra were collected with a Kratos AXIS Ultra system. The sample chamber was kept at was kept at < $5x10^{-9}$ torr. Ejected electrons are collected at an angle of 90º from the surface normal. Survey scans were performed to identify the elements on the surface of the carbon electrodes, with additional high resolution spectra collected for the transition metal elements of interest.

The XPS data were analysed using the program Computer Aided Surface Analysis for X-ray Photoelectron Spectroscopy (CasaXPS; from Casa Software Ltd., Teignmouth, UK). All XPS signals reported here are binding energies and are reported in eV. Backgrounds were fit with standard Shirley or linear backgrounds, while element peaks were fit with a standard Gaussian-Lorentzian line shape. For M 2p high resolution spectra, the major features were best fit as the $2p_{3/2}$ and $2p_{1/2}$ signals with constrained peak areas of 2:1 respectively.

Electrochemical experiments and methods

Electrochemical experiments were carried out in a N_2-filled glovebox in dry, degassed MeCN. 0.10 M tetra(n-butylammonium) hexafluorophosphate ($[nBu_4N]^+[PF_6]^-$; Oakwood Chemical, recrystallized from ethanol) served as the supporting electrolyte. Measurements were made with a Gamry Reference 600+ Potentiostat/Galvanostat using a standard three-electrode configuration. The working electrode was the basal plane of highly oriented pyrolytic graphite (HOPG) (GraphiteStore.com, Buffalo Grove, Ill; surface area: 0.09 cm^2),

the counter electrode was a platinum wire (Kurt J. Lesker, Jefferson Hills, PA; 99.99%, 0.5 mm diameter), and a silver wire immersed in electrolyte served as a pseudo-reference electrode (CH Instruments). The reference was separated from the working solution by a Vycor frit (Bioanalytical Systems, Inc.). Ferrocene (Sigma Aldrich; twice-sublimed) was added to an electrolyte solution prior to the beginning of each experiment; the midpoint potential of the ferrocenium/ferrocene couple (denoted as $Fc^{+/0}$) served as an external standard for comparison of the recorded potentials. Concentrations of analyte for cyclic voltammetry were 2 mM unless otherwise stated.

Piezeoelectric gravimetry

Electrochemical quartz crystal microbalance experiments were carried out in a N_2-filled glovebox. Measurements were made with a Gamry eQCM 10M electrochemical quartz crystal microbalance. Solutions were prepared in a static Teflon cell. An AT-cut quartz disk sputtered with gold and having a nominal resonant frequency of 10 MHz was used as the working electrode (Gamry Instruments; electroactive area ca. 0.205 cm^2). The counter electrode was a platinum wire (Kurt J. Lesker, Jefferson Hills, PA; 99.99%, 0.5 mm diameter), and a silver wire immersed in electrolyte served as a pseudo-reference electrode (CH Instruments). The reference was separated from the working solution by a Vycor frit (Bioanalytical Systems, Inc.)

Conflicts of interest

There are no conflicts to declare.

Acknowledgements

This work was supported by the US National Science Foundation through award CBET-1605524. X-ray photoelectron spectra were collected at the Molecular Materials Research Center in the Beckman Institute of the California Institute of Technology.

[1] (a) N. S. Lewis and D. G. Nocera, *Proc. Natl. Acad. Sci U. S. A.*, 2006, **103**, 15729. (b) N. S. Lewis, *Science*, 2016, **351**, 353. (c) M. G. Walter, E. L. Warren, J. R. McKone, S. W. Boettcher, Q. Mi, E. A. Santori and N. S. Lewis, *Chem. Rev.* 2010, **110**, 6446.

[2] (a) W. T. Eckenhoff, W. R. McNamara, P. Du and R. Eisenberg, *Biochim. Biophys. Acta Bioenerg.*, 2013, **1827**, 958. (b) J. R. McKone, S. C. Marinescu, B. S. Brunschwig, J. R. Winkler and H. B. Gray, *Chem. Sci.*, 2014, **5**, 865.

[3] M. Pourbaix, *Atlas of Electrochemical Equilibria in Aqueous Solutions*, Pergamon Press, 1966.

[4] D. C. Grills, D. E. Polyansky and E. Fujita, *ChemSusChem*, 2017, **10**, 4359-4373.

[5] J. D. Blakemore, N. D. Schley, G. W. Olack, C. D. Incarvito, G. W. Brudvig and R. H. Crabtree, *Chem. Sci.*, 2011, **2**, 94-98.

[6] (a) D. C. Lacy, G. M. Roberts and J. C. Peters, *J. Am. Chem. Soc.*, 2015, **137**, 4860. (b) V. Artero and M. Fontecave, *Chem. Soc. Rev.*, 2013, **42**, 2338. (c) E. S. Andreiadis, P.-A. Jacques, P. D. Tran, A. Leyris, M. Chavarot-Kerlidou, B. Jousselme, M. Matheron, J. Pécaut, S. Palacin, M. Fontecave and V. Artero, *Nat Chem*, 2013, **5**, 48-53.

[7] D. A. Buttry and M. D. Ward, *Chem. Rev.* 1992, **92**, 1355.

[8] N. D. Schley, J. D. Blakemore, N. K. Subbaiyan, C. D. Incarvito, F. D'Souza, R. H. Crabtree and G. W. Brudvig, *J. Am. Chem. Soc.*, 2011, **133**, 10473.

[9] D. J. Sconyers and J. D. Blakemore, *Chem. Commun.*, 2017, **53**, 7286.

[10] D. J. Sconyers and J. D. Blakemore, *Dalton Trans.*, 2019, **48**, 6372.

[11] B. J. Hathaway, D. G. Holah and A. E. Underhill, *J. Chem. Soc. (Resumed)*, 1962, 2444.

[12] J. Ke, W. Su, S. M. Howdle, M. W. George, D. Cook, M. Perdjon-Abel, P. N. Bartlett, W. Zhang, F. Cheng, W. Levason, G. Reid, J. Hyde, J. Wilson, D. C. Smith, K. Mallik and P. Sazio, *Proc. Natl. Acad. Sci. U. S. A.*, 2009, **106**, 14768.

[13] D. Cook, P. N. Bartlett, W. Zhang, W. Levason, G. Reid, J. Ke, W. Su, M. W. George, J. Wilson, D. Smith, K. Mallik, E. Barrett and P. Sazio, *Phys. Chem. Chem. Phys.*, 2010, **12**, 11744.

[14] A. M. Appel and M. L. Helm, *ACS Catal.*, 2013, **4**, 630.

[15] B. A. Lindquist, K. E. Furse and S. A. Corcelli, *Phys. Chem. Chem. Phys.*, 2009, **11**, 8119.

[16] P. Gans, A. Sabatini and L. Sacconi, *Inorg. Chem.*, 1966, **5**, 1877.

[17] A. Gavrikov, P. Koroteev, A. Ilyukhin, N. Efimov, A. K. Kostopoulos, A. Baranchikov, A. Tyurin, D. Kirdyankin, K. Gavrichev, F. Tuna and Z. Dobrokhotova, *Polyhedron*, 2017, **122**, 184.

[18] J. K. Clegg, J. Cremers, A. J. Hogben, B. Breiner, M. M. J. Smulders, J. D. Thoburn and J. R. Nitschke, *Chem. Sci.*, 2013, **4**, 68.

[19] N. Kuhn, H. Kotowski, C. Maichle-Mößmer and U. Abram, *Z. Anorg. Allg. Chem.*, 1998, **624**, 1653.

[20] A. K. Hijazi, A. Al Hmaideen, S. Syukri, N. Radhakrishnan, E. Herdtweck, B. Voit and F. E. Kühn, *Eur. J. Inorg. Chem.*, 2008, **2008**, 2892.

[21] I. Leban, D. Gantar, B. Frlec, D. R. Russell and J. H. Holloway, *Acta Cryst. C*, 1987, **43**, 1888.

[22] I. Søtofte, R. G. Hazell and S. E. Rasmussen, *Acta Cryst. B*, 1976, **32**, 1692.

[23] Y. Zhang, W. Sun, C. Freund, A. M. Santos, E. Herdtweck, J. Mink and F. E. Kühn, *Inorg. Chim, Acta*, 2006, **359**, 4723.

[24] J. M. Bąk, Effendy, S. Grabowsky, L. F. Lindoy, J. R. Price, B. W. Skelton and A. H. White, *CrystEngComm*, 2013, **15**, 1125.

[25] Y. Li, H. Y. Yeong, E. Herdtweck, B. Voit and F. E. Kühn, *Eur. J. Inorg. Chem.*, 2010, **2010**, 4587.

[26] J. Beck and M. Zink, *Z. Anorg. Allg. Chem.*, 2009, **635**, 687.

[27] S. F. Rach, E. Herdtweck and F. E. Kühn, *J. Organomet. Chem.*, 2011, **696**, 1817.

[28] W. E. Buschmann and J. S. Miller, *Chem. Eur. J.*, 1998, **4**, 1731.

[29] Savéant, J.-M. *Elements of Molecular and Biomolecular Electrochemistry*. Wiley: Hoboken, NJ, 2006.

[30] A. J. Bard, R. Parsons and J. Jordan, *Standard Potentials in Aqueous Solution*, M. Dekker, New York, 1985.

[31] V. V. Pavlishchuk and A. W. Addison, *Inorg. Chim. Acta*, 2000, **298**, 97.

[32] A. J. Bard and L. R. Faulkner, *Electrochemical Methods: Fundamentals and Applications*, Wiley, Hoboken, NJ, 2nd edn, 2001.

[33] I. Favier and E. Duñach, *Tetrahedron Lett.*, 2004, **45**, 3393.

[34] J. T. Muckerman, J. H. Skone, M. Ning and Y. Wasada-Tsutsui, *Biochim. Biophys. Acta Bioenerg.*, 2013, **1827**, 882-891.

[35] G. Sauerbrey, *Z. Phys.*, **1959**, *155*, 206.

[36] J. F. Moulder, W. F. Stickle, P. E. Sobol and K. D. Bomben, *Handbook of X-ray Photoelectron Spectroscopy*, Perkin-Elmer Corp., 1992.

[37] D. N. Hendrickson, J. M. Hollander and W. L. Jolly, *Inorg. Chem.*, 1969, **8**, 2642-2647.

TOC Graphic

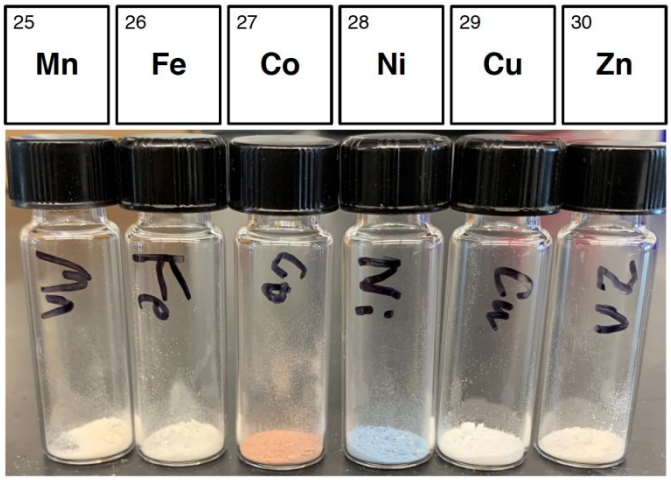

Properties of homoleptic acetonitrile complexes:
Electrodeposition, anodic stripping, and chemical corrosion

Homoleptic first-row transition metal acetonitrile complexes are shown to be precursors for metal electrodeposition from homogeneous solutions.